arXiv:1106.0578v1 [astro-ph.CO] 3 Jun 2011

Mon. Not. R. Astron. Soc. **000**, 1–11 (2011) Printed 27 January 2013 (MN LATEX style file v2.2)

On the absence of molecular absorption in high redshift millimetre-band searches

S. J. Curran[1]⋆, M. T. Whiting[1,2], F. Combes[3], N. Kuno[4], P. Francis[5], N. Nakai[6], J. K. Webb[1], M. T. Murphy[1,7] and T. Wiklind[8,9,10]

[1]*School of Physics, University of New South Wales, Sydney NSW 2052, Australia*
[2]*CSIRO Australia Telescope National Facility, PO Box 76, Epping NSW 1710, Australia*
[3]*LERMA, Observatoire de Paris, France*
[4]*Nobeyama Radio Observatory, Nagano 384-1305, Japan*
[5]*Australian National University, Australia*
[6]*Institute of Physics, University of Tsukuba, Ten-noudai, Tsukuba, Ibaraki 305-8571, Japan*
[7]*Centre for Astrophysics and Supercomputing, Swinburne University of Technology, PO Box 218, Hawthorn, VIC 3122, Australia*
[8]*Space Telescope Science Institute, USA*
[9]*Onsala Space Observatory, S-439 92 Onsala, Sweden*
[10]*Joint ALMA Observatory, Santiago, Chile*

Accepted —. Received —; in original form —

ABSTRACT

We have undertaken a search for millimetre-wave band absorption (through the CO and HCO$^+$ rotational transitions) in the host galaxies of reddened radio sources ($z = 0.405 - 1.802$). Despite the colour selection (optical–near infrared colours of $V - K \gtrsim 5$ in all but one source), no absorption was found in any of the eight quasars for which the background continuum flux was detected. On the basis of the previous (mostly intervening) H_2 and OH detections, the limits reached here and in some previous surveys should be deep enough to detect molecular absorption according to their $V - K$ colours. However, our survey makes the assumption that the reddening is associated with dust close to the emission redshift of the quasar and that the narrow millimetre component of this emission is intercepted by the compact molecular cores. By using the known millimetre absorbers to define the *colour depth* and comparing this with the ultra-violet luminosities of the sources, we find that, even *if* these assumptions are valid, only twelve of the forty objects (mainly from this work) are potentially detectable. This is assuming an excitation temperature of $T_{\mathrm{x}} = 10$ K at $z = 0$, with the number decreasing with increasing temperatures (to zero detectable at $T_{\mathrm{x}} \gtrsim 100$ K).

Key words: radio lines: galaxies – galaxies: active – quasars: absorption lines – cosmology: observations – galaxies: abundances – galaxies: high redshift

1 INTRODUCTION

Millimetre-wave observations of molecular absorption systems along the sight-lines to distant quasars provide a powerful probe of the cold, dense, star forming gas in the distant Universe. Furthermore, comparison of the redshifts of the rotational transitions of the molecules with those of the spin-flip transition of H I, as well as the electronic optical/UV transitions of metal ions, can be used to determine high redshift values of the fundamental constants, to at least an order of magnitude the sensitivity of purely optical data (see Curran et al. 2004a). However, despite much searching, only four such systems are currently known (Wiklind & Combes 1995, 1996a,b, 1997), the highest redshift being at $z_{\mathrm{abs}} = 0.89$. Of these, two are intervening systems (gravitational lenses towards more distant quasars), with the other two systems arising through absorption within the host galaxy of the quasar. Subsequent searches at the redshifts of known high column density H I absorption systems, intervening the sight-lines to more distant quasi-stellar objects (QSOs), have also failed to detect molecular absorption in the millimetre-band (Curran et al. 2004b and references therein), despite the possibility that these so-called damped Lyman-α systems (DLAs)[1] may account for more than 80 per-cent of the neutral gas content in the Universe (Prochaska et al. 2005).

DLAs are, however, not devoid of molecular gas: To date, the Lyman and Werner ultra-violet bands of H_2 have been detected in

---

[1] These have neutral hydrogen column densities of $N_{\mathrm{HI}} \geqslant 2\times10^{20}$ cm^{-2} and are usually detected at $z_{\mathrm{abs}} \gtrsim 1.8$, where the Lyman-$\alpha$ transition is redshifted in to the optical band.

⋆ E-mail: sjc@phys.unsw.edu.au

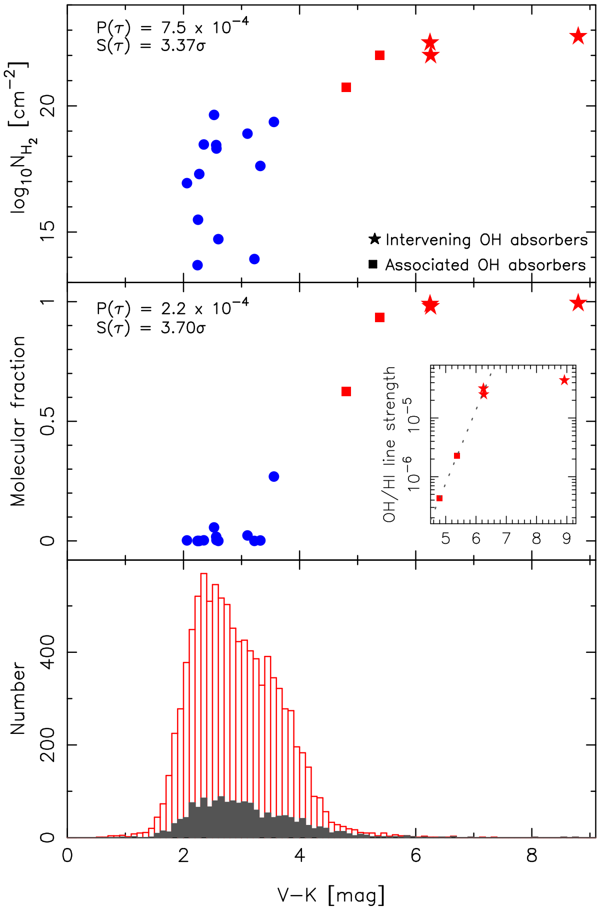

Figure 1. The H_2 column density (top) and the molecular fraction (middle) versus the observed frame optical–near infrared colour (where available) for high redshift molecular absorption systems. The circles represent the H_2-bearing DLAs (all optically selected intervening absorbers) and the squares and stars the OH absorbers (radio selected), with the inset in the middle panel showing the normalised OH line strength (Curran et al. 2006). These are comprised of the four systems originally identified in millimetre-wave transitions (with the least-squares fit to these shown) plus the gravitational lens at $z_{\rm abs} = 0.764$ towards 0132–097 (detected in OH decimetre but not HCO^+ millimetre absorption, Kanekar et al. 2005). $P(\tau)$ shows Kendall's τ two-sided probability of the observed distribution occuring by chance and $S(\tau)$ the significance of this assuming Gaussian statistics. The bottom panel shows the distribution of SDSS quasars (Schneider et al. 2007, after conversion to V magnitudes, Fukugita et al. 1996) where the filled histogram shows those which have been detected in the Very Large Array's "Faint Images of the Radio Sky at Twenty Centimetres" (FIRST) survey (Becker et al. 1995).

19 DLAs (see Noterdaeme et al. 2008[2], Jorgenson et al. 2009 and Srianand et al. 2010). These, however, have molecular abundances which are generally much lower than those detectable with current microwave and radio telescopes (Curran et al. 2004b and Fig. 1, top). Furthermore, in Curran et al. (2006) we showed that the H_2-bearing DLAs have molecular fractions of $\mathcal{F} \equiv \frac{2N_{\rm H_2}}{2N_{\rm H_2}+N_{\rm HI}} \sim 10^{-7} - 0.3$ and $V-K \lesssim 4$ (Fig. 1, middle), i.e. in the same range as a "typical" QSO (Fig. 1, bottom)[3], whereas the millimetre and decimetre band absorbers have molecular fractions $\mathcal{F} \approx 0.6 - 1$ and optical–near-infrared colours of $V - K \gtrsim 5$.

The correlations in Fig. 1 present strong evidence that the quasar light is reddened by dust in the foreground absorber: Since the presence of the dust is necessary to prevent the dissociation of the molecular gas by the ambient ultra-violet field, the molecular fraction is expected to be correlated with the dust abundance, as observed. The paucity of millimetre-wave band absorption can therefore be attributed to the traditional optical selection of targets biasing towards absorbers of low dust content and therefore low molecular fractions.

The fact that intervening absorbers are usually found through optical spectroscopy, yielding a redshift but also giving the above bias against dusty objects, means that millimetre-band searches of known intervening absorbers have generally been unsuccessful (Curran et al. 2004b and references therein). An alternative target for molecular absorption is towards the fainter "red quasars", where the red colour may indicate an intervening column of dust. However, due to the relatively narrow bandwidths in the millimetre band (see Sect. 4.2), such an approach is currently only practical at longer (decimetre) wavelengths (see Curran et al. 2011b). In the absence of any known intervening absorbers, selecting the quasar itself gives a redshift ($z_{\rm em}$) to which to tune the receiver. Naturally, such a selection of targets prevents any useful comparison with the optical redshifts, in order to measure the values of the fundamental constants, although any detections could be followed up in 21-cm, giving the redshift of the spin-flip transition of H I.

In Curran et al. (2006, 2008, 2011a), we presented the results from our decimetre-wave searches for such "associated" (OH and H I) absorption and here present the results of our millimetre-wave survey for associated absorption.

2 OBSERVATIONS

2.1 Target selection

As per Curran et al. (2006), our sources were selected from the Parkes Half-Jansky Flat-spectrum Sample (PHFS, Drinkwater et al. 1997)[4], on the basis of their optical–near-IR photometry (Francis et al. 2000). From these, we selected the 30 reddest sources (which correspond to an extinction of $A_V \approx 4.1$), in which the emission redshift of the quasar ($z_{\rm em}$) would place a strong absorption line (CO or HCO^+) into the 3-mm band. After culling these further, by selecting those of $\delta > -30^\circ$ (thus being observable from northern latitudes)[5] and with 3-mm flux densities expected to be $\gtrsim$ 100 mJy, the ten objects listed in Table 3.1 remained.

2.2 The IRAM 30-m observations

From December 2003 to February 2004 we observed three of the targets with the IRAM (Institut de Radio Astronomie Millimetrique) 30-m telescope at Pico Veleta, Spain. We used two 3-mm SIS receivers (A100 and B100), tuned to the redshifted frequencies of the molecular transitions (see Table 3.1). The observations were done with a nutating subreflector, switching symmetrically $\pm 90''$ in azimuth with a frequency of 0.5 Hz. The continuum levels of the observed sources were determined using a continuum backend and increasing the subreflector switch frequency to 2 Hz. The image sideband rejection of the receivers were high, of the order of 20 dB (single sideband). System temperatures typically ranged from 120 K (90 GHz) to 180 K (113 GHz). We used the full 1 GHz backend with broad (1MHz) filterbanks and narrow band autocorrelators, the former giving a channel spacing of $\approx 3-4~{\rm km~s^{-1}}$ (Table 3.1) over a bandwidth of $\approx 1500~{\rm km~s^{-1}}$, which should be sufficient to cover uncertainties in the emission redshifts, all of which are known to at least three decimal places ($\Delta z = \pm 0.001$ corresponds to $\Delta v \approx \pm 100 - 200~{\rm km~s^{-1}}$ for our sample). The pointing of the telescope was checked regularly on nearby continuum sources. Typical pointing corrections were $5-10''$. The focus was checked regularly on Mars and Saturn. The Half Power Beam Width (HPBW) at 95 GHz is $26''$.

---

[2] One of which, J1439+113, has also been detected in the CO $A - X$ UV band (Srianand et al. 2008).

[3] $V - K = 2.88 \pm 1.04$ in general and 3.05 ± 0.97 if radio-loud.

[4] With the addition of 0500+019, included since it has been detected in 21-cm absorption (Carilli et al. 1998). We also included J0906+4952 & J1341+3301, which are two very red sources from Glikman et al. (2004) [Sect. 2.3].

[5] We miss SEST.

We prioritised the three targets according to the 3-mm flux densities estimated from an interpolation of the decimetre and near-infrared values: 12.8 hours of integration on 0500+019 ($S_{\rm est} \approx 0.32$ Jy), 13.6 hours on 1430–155 ($S_{\rm est} \gtrsim 0.08$ Jy) and 7.2 hours on 1504–166 ($S_{\rm est} \gtrsim 0.8$ Jy), which, upon comparison with the observed values (Table 3.1), were reasonable estimates. The data were reduced with the GILDAS[6] software package.

2.3 The NRO 45-m observations

The remainder of the sample was observed with the Nobeyama Radio Observatory's 45-m telescope in March 2004. We used the H28/32 (1-cm) and the S80, S100 (3-mm) receivers to observe the $J = 0 \to 1$ and $1 \to 2$ transitions over a range of redshifts (Table 3.1). The observations were performed in position switching mode, with an integration time of 20 s for each scan. The antenna temperature, $T_{\rm A}^*$, was obtained by the chopper-wheel method, which corrected for atmospheric and ohmic losses. System temperatures typically ranged from 200 K (1-cm) to 500 K (3-mm). We used the AOS backend over 250 MHz split over 2048 channels, which gave channel spacings of 0.37 (3-mm) ${\rm km~s^{-1}}$ to 1.1 ${\rm km~s^{-1}}$ (1-cm) with bandwidths of ≈ 700 and $\approx 2000~{\rm km~s^{-1}}$, respectively. The pointing of the telescope was checked by observing SiO maser sources with the H40 (40 GHz band) receiver and the corrections were $\leqslant 10$".

The 3-mm observations were performed when the weather was clearest, with total integration times of 2 hours for 0213–026, 5 hours for 0454+066, 3.7 hours for 1107–187 and 8.5 hours for 1706+006 (for which we could not determine the flux density, Fig. 2)[7]. During less than ideal weather conditions, we observed in the 1-cm band and included the radio detected, optically dim sources of Glikman et al. (2004), where HCO$^+$ $0 \to 1$ is redshifted into this band — the FIRST–2MASS reddened quasars J0906+4952 (SDSS J090651.49+495235.9) and FTM J1341+3301. The data were reduced with the NEWSTAR package and, like the IRAM results, upon the removal of a low order baseline and smoothing no absorption features were apparent in the spectra.

3 RESULTS

3.1 Observational results

In Fig. 2 we show the reduced spectra and in Table 3.1 we summarise our observational results. The limit to the total column density of each molecule is calculated from

$$N_{\rm total} = \frac{8\pi}{c^3}\frac{\nu^3}{g_{J+1}A_{J+1\to J}}\frac{Q e^{E_J/kT_{\rm x}}}{1-e^{-h\nu/kT_{\rm x}}}\int \tau dv, \qquad (1)$$

where ν is the rest frequency of the $J \to J+1$ transition, g_{J+1} and $A_{J+1\to J}$ are the statistical weight and the Einstein A-coefficient of the transition, respectively, and $Q = \sum_{J=0}^{\infty} g_J~e^{-E_J/kT_{\rm x}}$ is the partition function[8]. In the case of the four known systems, the covering factor is expected to be close to unity (Wiklind & Combes 1994, 1995, 1996b, 1998) so, as in the optically thin regime, this can be written outside of the integral. However, unlike lower frequency searches (e.g. OH 18-cm, $^2\Pi_{3/2}$), in the millimetre regime even low excitation temperatures give $kT_{\rm x} \sim E_J \sim h\nu$ and so the column density cannot be approximated via a linear dependence on this. Therefore, unlike the decimetre searches for associated absorption (Curran et al. 2006, 2008, 2011a), we must assume an excitation temperature.

In Table 2 we apply Equation 1 to the velocity integrated optical depths given in the references in order to derive the column densities and excitation temperatures of the four known systems. These are found to be close to those derived by Wiklind & Combes (1995, 1996a,b, 1997) and so for our targets we adopt an excitation temperature of $T_{\rm x} = 10$ K at $z = 0$.

Although the excitation temperatures are similar, the four known millimetre absorbers exhibit a range of full-width half maxima (FWHMs), ranging from FWHM$\approx~2~{\rm km~s^{-1}}$ (1413+135, Wiklind & Combes 1997) to $\approx~70~{\rm km~s^{-1}}$ (the main component towards 1504+377, Wiklind & Combes 1996b). For these, plus the absorber towards 0132–097 (Sect. 1), it has been shown that the OH 18-cm ($^2\Pi_{3/2} J = 3/2$) FWHMs are similar to those of the H I 21-cm profiles (Curran et al. 2007), although we cannot yet unambiguously state that millimetre widths are correlated with those of the decimetre lines (Fig. 3). In any case, of all of our targets, only one (0500+019) has been detected in 21-cm absorption (see table 6 of Curran et al. 2008 and Sect. 4.2), and so we would have no information on what the width of each of the undetected lines should be. If this were known, we would smooth the spectral resolution (Δv) of the data to the FWHM of the line, thus giving the best possible optical depth limit, based upon the detection of absorption in a single channel. Multiplying the resulting optical depth, scales the velocity integrated optical depth to $\tau \times {\rm FWHM}/\Delta v$, giving an overall scaling of $\sqrt{{\rm FWHM}/\Delta v}$.

Choosing either the minimum and maximum FWHM of the four known absorbers, therefore gives a possible range in scaling factors of $\sqrt{70/2} \approx 6$, and so the choice of either FWHM$\approx~2~{\rm km~s^{-1}}$ or $\approx~70~{\rm km~s^{-1}}$ could lead to a significant over/under-estimate in the profile width. We therefore use the optical–near-infrared colour, which appears to be correlated with the profile

---

[6] http://www.iram.fr/IRAMFR/GILDAS/

[7] The highest frequency flux measurement available for 1706+006 is 0.44 Jy at 5.0 GHz (Wright & Otrupcek 1990).

[8] The Einstein A-coefficients are taken from Chandra et al. (1995, 1996) or derived from the permanent electric dipole moment of the molecule, obtained from the JPL Spectral Line Catalog (Pickett et al. 1998), along with the energy of each level, E_J. An on-line column density calculator based on Equation 1 is available from http://www.phys.unsw.edu.au/∼sjc/column/

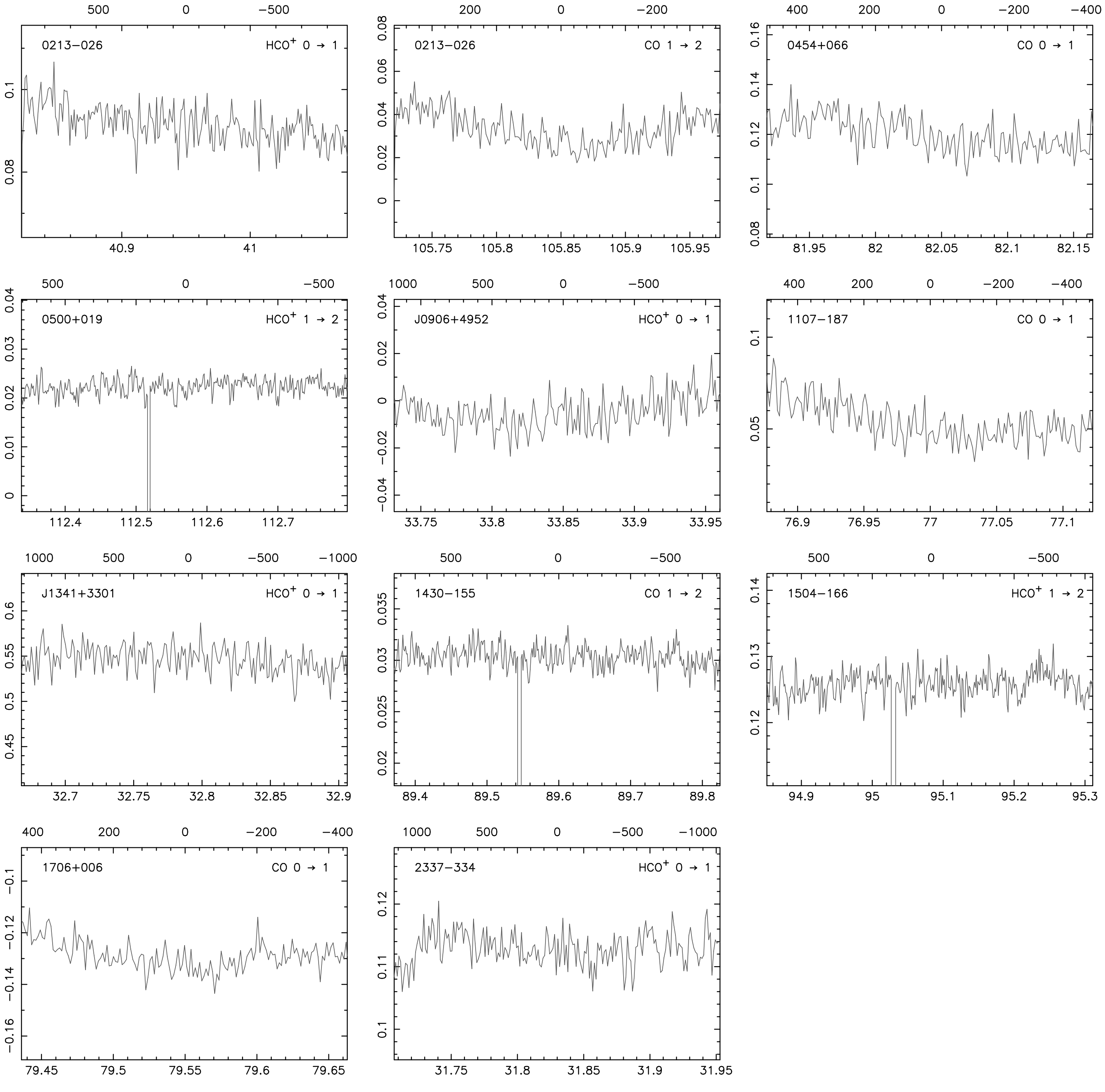

Figure 2. The observed spectra before baseline removal. The ordinate in each spectrum shows the antenna temperature in $T_{\rm A}^*$ [K] and the abscissa the barycentric frequency [GHz], with the top axis showing the velocity offset from the central tuned frequency [$\rm km\,s^{-1}$]. All are shown at a resolution of $4\ \rm km\,s^{-1}$, the coarsest of the observations (see Table 3.1). The negative spike in each of the IRAM spectra are due to bad channels (246–250) and the negative flux for 1706+006 is due to the long (20 s) integrations with the NRO giving errors in the continuum flux measurement.

Table 2. The excitation temperatures and column densities derived from the listed references. In the case where the T_x entry is empty, the column density is calculated at the excitation temperature of the other molecule.

System	$z_{\rm abs}$	Reference	CO		HCO$^+$	
			T_x [K]	$N_{\rm total}$ [cm^{-2}]	T_x [K]	$N_{\rm total}$ [cm^{-2}]
0218+357	0.68466	Wiklind & Combes (1995)	9	$6.3 \pm 0.3 \times 10^{16}$	–	$5.1 \pm 0.2 \times 10^{13}$
1413+135	0.24671	Wiklind & Combes (1997)	–	$1.54 \pm 0.04 \times 10^{16}$	8	$2.4 \pm 0.4 \times 10^{13}$
1504+377	0.67335	Wiklind & Combes (1996b)	16	$5.9 \pm 1.0 \times 10^{16}$	13	$6.5 \pm 0.1 \times 10^{13}$
1830−211	0.88582	Wiklind & Combes (1996a, 1998)	–	$\approx 6 \times 10^{17}$	8	$2.9 \pm 0.3 \times 10^{14}$

Table 1 The search results. $V-K$ is the optical–near-infrared colour (see Curran et al. 2006, 2008 and references therein and Glikman et al. 2004), $z_{\rm em}$ is the emission redshift of the target, "Tel." gives the telescope used with the total integration time in hours, $t_{\rm int}$, followed by the transition searched along with the central tuned frequency [GHz]. $\sigma_{\rm rms}$ is the r.m.s. noise [mK] reached per Δv channel [km s^{-1}] and $T_{\rm cont}$ is the continuum measured in $T_{\rm A}^{*}$ [mK]. This is converted to a flux density $S_{\rm cont}$ [Jy], using a conversion of 6 Jy per K for the IRAM 30-m at 3-mm and $\eta_{\rm mb} = 0.79$ (32 GHz), 0.77 (43 GHz), 0.51 (86 GHz) & 0.52 (100 GHz) for the NRO 45-m. $\tau = -\ln(1 - 3\sigma_{\rm rms}/T_{\rm cont})$ is the optical depth limit of the relevant millimetre line calculated from the r.m.s. noise per estimated FWHM, except for 0454+066 and J1341+3301, which are 2 and 70 km s^{-1}, respectively (see main text). $N_{\rm total}$ [cm^{-2}] is the total column density per channel of the relevant molecule obtained from this (for an excitation temperature of $T_{\rm x} = 10$ K at $z = 0$, see main text) over the redshift range quoted.

Source	$V-K$	$z_{\rm em}$	Tel.	$t_{\rm int}$	Transition	$\nu_{\rm obs}$	$\sigma_{\rm rms}$	Δv	$T_{\rm cont}$	$S_{\rm cont}$	$\tau\,(3\sigma)$	$N_{\rm total}$	z range
0213–026	5.65	1.178	NRO	10.4	HCO$^+$ $0\rightarrow1$	40.95	5.9	0.9	91	0.24	<0.058	$<7.8\times10^{12}$	1.1712 – 1.1848
...	...	...	NRO	2.0	CO $1\rightarrow2$	105.85	12	0.37	33	0.13	<0.23	$<1.1\times10^{16}$	1.1754 – 1.1806
0454+066	4.32	0.405	NRO	5.0	CO $0\rightarrow1$	82.04	10	0.45	120	0.48	<0.13	$<1.8\times10^{15}$	0.4028 – 0.4072
0500+019	5.75	0.58457*	IRAM	12.8	HCO$^+$ $1\rightarrow2$	112.57	1.6	3.4	23	0.14	<0.11	$<6.3\times10^{12}$	0.5811 – 0.5882
J0906+4952	5.68	1.635	NRO	2.2	HCO$^+$ $0\rightarrow1$	33.85	12	1.1	<12	<0.03	—	—	1.6251 – 1.6450
1107–187	5.15	0.497	NRO	3.7	CO $0\rightarrow1$	77.00	16	0.51	54	0.21	<0.38	$<1.1\times10^{16}$	0.4945 – 0.4995
J1341+3301	7.19	1.720	NRO	1.1	HCO$^+$ $0\rightarrow1$	32.79	25	1.1	550	1.41	<0.017	$<1.8\times10^{13}$	1.7094 – 1.7307
1430–155	5.74	1.573	IRAM	13.6	CO $1\rightarrow2$	89.60	1.0	4.2	31	0.18	<0.057	$<3.5\times10^{15}$	1.5658 – 1.5802
1504–166	5.74	0.876	IRAM	7.2	HCO$^+$ $1\rightarrow2$	95.08	1.9	3.9	126	0.76	<0.025	$<1.5\times10^{12}$	0.8711 – 0.8810
1706+006	4.96	0.449	NRO	8.5	CO $0\rightarrow1$	79.55	7.8	0.48	—	—	—	—	0.4467 – 0.4513
2337–334	5.50	1.802	NRO	12.9	HCO$^+$ $0\rightarrow1$	31.83	4.4	1.2	113	0.29	<0.045	$<2.9\times10^{12}$	1.7908 – 1.8133

Notes: *The mean redshift of the H I 21-cm absorption detected by Carilli et al. (1998) which has two components, giving a total column density of $N_{\rm HI} = 6.2\times10^{18}.(T_{\rm s}/f)$ cm^{-2}.

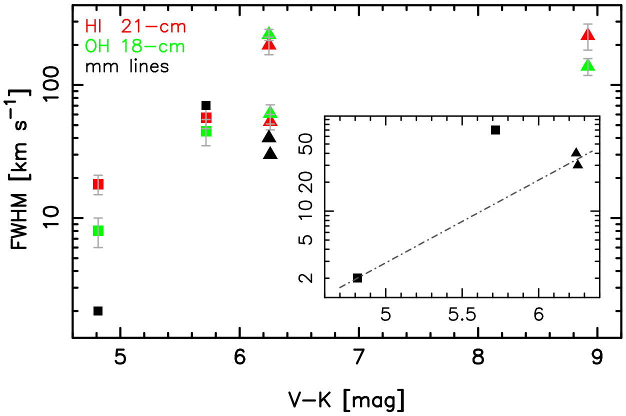

Figure 3. The FWHM of the H I and OH profiles versus the optical–near-infrared colour for the five OH absorbers. The black symbols show the approximate millimetre FWHM versus the optical–near-infrared colour, for the four of the five detected in millimetre lines,. The inset shows the millimetre detections only with the line showing the fit used to estimate the FWHM for our targets.

width in the four known systems (Fig. 3)[9], in order to estimate what the FWHM of an undetected absorber should be.

As seen from the figure, the associated absorber in 1504+377 represents a stray point with a FWHM of ≈ 70 km s^{-1}. We therefore estimate the profile widths from the least-squares-fit to the other three systems (shown in the inset of Fig. 3). The fact that this is based upon only three points, with the removal of one which we simply do not like, limits the robustness of this method, although it should give a better handle on the profile width than a simple assumption. We therefore use this fit, $\log_{10}{\rm FWHM} \approx 0.86\,(V-K) - 3.84$ (for $2 \leqslant {\rm FWHM} \leqslant 70$ km s^{-1}), to estimate the column density limits (given in Table 3.1).[10]

3.2 Comparisons with the known high redshift molecular absorbers

In Fig. 4 we show the CO and HCO$^+$ column densities normalised by that of the H I 21-cm (from Carilli et al. 1992, 1993, 1998; Chengalur et al. 1999) against the optical–near-IR colour, for the four known millimetre absorbers. From this it is difficult to ascertain whether there is a correlation between the normalised millimetre-wave column density and the $V-K$ colour, as is found for the normalised OH column densities in Curran et al. (2006) [Fig. 1]. Furthermore, 21-cm line strengths are not available for the sample although in Curran et al. (2006) there was still a, albeit more scattered, correlation between the un-normalised OH $^2\Pi_{3/2}J = 3/2$ column density and the $V-K$ colour, which appears to apply to all of the molecular absorbers (Fig. 1, top). Therefore in Fig. 5 we show the un-normalised CO and HCO$^+$ column densities against the colour for our targets, as well as those from previous searches of associated molecular absorption (Wiklind & Combes 1995, 1996b;

---

[9] This suggests that the path length through the dust responsible for the reddening may be correlated with the orientation of a rotating cloud complex, such as the disk of a galaxy (Curran & Whiting, in prep.). There is a 1% probability of this correlation arising by chance (for H I, Fig. 3), i.e. a 3.30σ significance assuming Gaussian statistics.

[10] In order to guard against over-compensating, we use the minimum and maximum observed profile widths of 2 and 70 km s^{-1} in cases where the estimated FWHMs are less or greater than these limiting values.

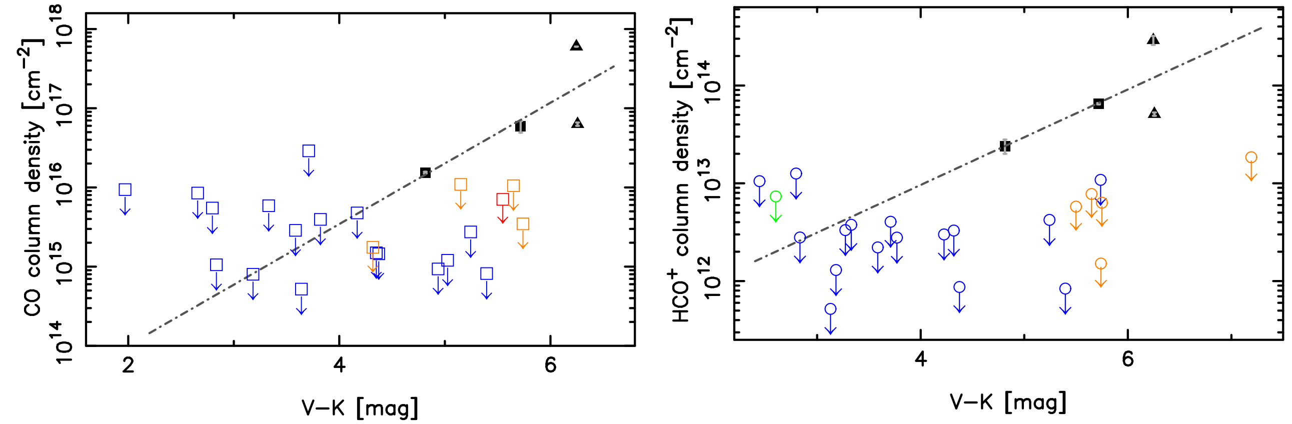

Figure 5. The CO (left) and HCO$^+$ (right) column densities versus optical–near-IR colour. The symbols are as per Fig. 4, with the filled symbols showing the four known systems (the line shows the least-squares fit to these) and the unfilled symbols showing the limits from the searches by Wiklind & Combes (1995, 1996b); Drinkwater et al. (1996) [blue] Murphy et al. (2003) (specifically 0727–115 at $z_{\rm em} = 1.591$, see Sect. 4.2) [red] and the millimetre wave searches of Curran et al. (2006) [green] (actually HCN in 0335–122, since this is the only source for which V and K are available) and this paper [orange]. All of the limits are at the 3σ level per channel recalculated for the expected FWHM, except when outside the range of the four known, where either 2 or 70 km s^{-1} is used (Sect. 3.1). Note that this range may add a potential uncertainty of 0.78 dex to the column density estimates (Sect. 3.1, although see footnotes 12 and 13), in addition to further uncertainty from the assumption of $T_{\rm x} = 10$ K at $z = 0$ (see Sect. 4.3).

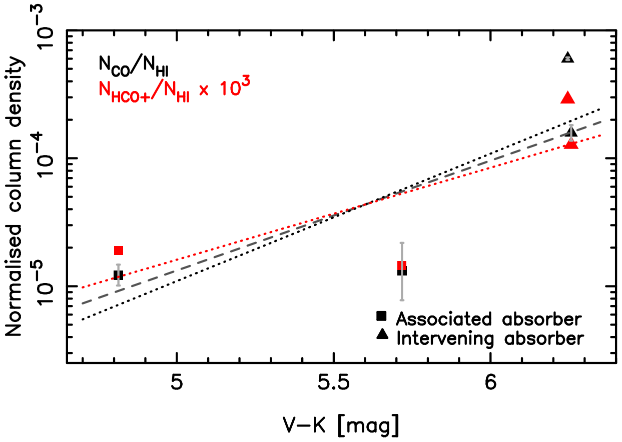

Figure 4. The normalised (assuming $T_{\rm s}/f = 100$ K) CO (black) and HCO$^+$ (coloured) column densities versus optical–near-IR colour. The dotted lines show the least-squares fit for each of the molecules with the dashed line showing the composite fit.

Drinkwater et al. 1996; Murphy et al. 2003; Curran et al. 2008).[11] From these, we see that many of the limits (especially the new ones reported in this paper, shown in orange), should be more than sufficient to detect molecular absorption, particularly HCO$^+$. Incorporating the upper limits of the column densities, via the ASURV survival analysis package (Isobe et al. 1986), gives Kendall's τ two-sided probabilities of $P(\tau) = 0.0092$ ($n = 26$) [i.e a significance of $S(\tau) = 2.60\sigma$ for CO][12] and $P(\tau) = 0.025$ ($n = 27$) [$S(\tau) = 2.24\sigma$ for HCO$^+$][13] of the column density–colour correlations occuring by chance. For the five known OH absorbers, $S(\tau) = 1.96\sigma$ (Curran et al. 2011a), which falls to 1.36σ for those four detected in millimetre transitions.[14] So although the search results do not lessen the significance of the column density–colour correlations (but actually increase them), many of the limits are below those expected for a detection and so we discuss other possible reasons as to why millimetre-wave spectral lines were undetected in this and the previous surveys.

4 DISCUSSION: POSSIBLE EXPLANATIONS FOR THESE AND THE PREVIOUS NON-DETECTIONS

4.1 Millimetre-wave covering factors

While there is an apparent correlation between the normalised column density and the optical–near infrared colour, Fig. 1 actually shows the ratio of the OH 18-cm velocity integrated optical depth to that of the H I 21-cm. Therefore in order for the fit to be accurate for the normalised column densities, the four known millimetre absorbers must also have similar spin and excitation temperatures, as well as H I and OH covering factors (or at least a similar ratio of these quantities). While the excitation temperatures can be well constrained from the millimetre transitions (Table 2) and the spin temperatures can be removed by not normalising the column densities (Fig. 4 cf. 5), the covering factor, f, is ingrained into the optical depth via, $\tau = -\ln\left(1 - \frac{\sigma}{f\,S}\right)$. Since the CO and HCO$^+$ lines are optically thick in the four known systems, $-\ln\left(1 - \frac{\sigma}{f\,S}\right) \neq \frac{\sigma}{f\,S}$, thus not allowing f to be taken outside of the integral in Equation 1, although, as noted in Sect. 3.1, if $f \approx 1$ this would have little effect.

In any case, the correlation shown in Fig. 4 does not hold for *all five* of the absorbers: Towards the $z_{\rm em} = 2.215$ quasar PMN J0134–0931 (0132–097), Kanekar et al. (2005) detected OH at a column density of $N_{\rm OH} = 5.6 \times 10^{14}.\,(T_{\rm x}/f)$ cm^{-2} in the intervening $z_{\rm abs} = 0.765$ gravitational lens, although HCO$^+$ $1 \rightarrow 2$ was undetected to $\tau < 0.07$. This gives a column density ratio of $N_{\rm OH} \gtrsim 5600 N_{\rm HCO^+}$. Curran et al. (2007) have suggested that the non-detection of millimetre absorption towards 0132–097 could be a geometrical effect, where a molecular cloud has a much larger chance of occulting the lower frequencies, since the decimetre emission region is likely to be much larger than the millimetre region (as may also be exhibited by the wider decimetre profiles, Fig. 3). That is, the narrower millimetre emission is less likely to intercept the CO and HCO$^+$ gas which will be localised in dense molecular cores. The fact that the millimetre and decimetre emission, and thus absorption, trace different components of the gas could be responsible for the significance of the correlation with colour not changing when normalising the millimetre column densities by that of the H I (Sect. 3.2).

---

[11] In the plots we give Wiklind & Combes (1995, 1996b); Drinkwater et al. (1996) the same colour as the latter paper includes some of the results of the first two.

[12] Bearing in mind that these limits are subject to the FWHM estimates (Sect. 3.1), we have also derived the probabilities when applying the two FWHM extrema of the detected absorbers, 2 and 70 km s^{-1}. Not generally being as red as the detected sample, the values do not change for FWHM= 2 km s^{-1}, and for 70 km s^{-1}, $P(\tau)_{70} = 0.0075$ & $S(\tau)_{70} = 2.68\sigma$ ($n = 28$).

[13] Again, applying FWHM= 2 km s^{-1} introduces no change to the correlation and $P(\tau)_{70} = 0.022$ & $S(\tau)_{70} = 2.29\sigma$ ($n = 30$).

[14] $S(\tau) = 2.25\sigma$ for the five known OH absorbers plus the OH limits (Curran et al. 2011a).

In the case of 0132–097 , the possibility that the core of the absorbing molecular gas is offset from the centre of the emission may also result in a reduction of the decimetre covering factor, which could be the cause of the normalised OH line strength in 0132–097 not being as high as expected from its colour (i.e. below the fit defined by the others in Fig. 1, right), although more absorbers would be required to verify this.

4.2 Location of the absorbing gas

From the fact that, of our sample, H I has only been detected in 0500+019[15] we may be incorrect in our assumption that the host galaxy is generally the location of the quasar reddening, as it is for only two of the five known OH absorbers. As is the case for the remaining three of the known systems, the absorption (and thus the cause of the reddening) could be occuring anywhere between us and the emission redshift of the quasar. Unfortunately, full range spectral scans are not feasible towards most sources with current instruments and, over the ranges which are scanned, there is a trade-off between the redshift space which can be covered and the depth of the search. Thus our motivation for searching for molecular absorption within the host galaxy. Spectral scans have, however, been attempted (Murphy et al. 2003; Curran et al. 2005), with 0500+019 being one of the targets common to ours. We summarise the results in Table 3, from which we see that $< 30\%$ of the redshift space towards 0500+019 has been scanned for HCO$^+$ and only 12% for CO, with some overlap in these ranges. We therefore cannot rule out that the cause of the reddening may be at some other redshift towards 0500+019 and indeed for the rest of the sample.

There is also the possibility that, even if the reddening (and hence any absorption) is located at the host, it would only be detected if the optical redshift is known precisely enough to ensure that the observed band covers the correct redshift range. The optical spectra of these quasars have spectral resolutions of $\approx 5-8$ Å, which corresponds to a few hundred km s^{-1}, which is close to our observed bandwidths (Fig. 2). However, most of the quasars observed here have have strong narrow emission lines, which constrain the redshift to better than $\sim 10^{-4}$ and all are quoted to at least the third decimal place, although uncertainties are usually not given (Drinkwater et al. 1997). Referring to the ranges covered by our observed bands (Table 3.1), we see that offsets of $\Delta z \approx \pm 0.002$ (at low redshifts) to $\approx \pm 0.01$ (at high redshifts) are covered, thus making it unlikely that our observations are generally tuned to the wrong frequency.

4.3 Conditions within the host

Above we suggest the possibility that molecular absorption is not detected since the reddening of the quasar light may not necessarily be occuring close to the redshift of the background quasar. Over and above this, there is the possibility that a large column of absorbing molecular gas *cannot* be located in the host galaxy on the basis that the there is a low fraction of cool neutral gas in the hosts of quasars and radio galaxies with ultra-violet luminosities of $L_{\rm UV} \gtrsim 10^{23}$ W Hz^{-1} (Curran et al. 2008). Whether this is due to excitation of the gas or these luminosities selecting gas-poor ellipticals (or indeed whether these two possibilities are inter-related, Curran & Whiting 2010), this appears to be the case for *all* redshifted ($z_{\rm em} \gtrsim 0.1$) H I 21-cm absorption searches.

In order to investigate whether this could affect our sample, we use the photometry of the searched sources (Table 4) to derive the UV luminosities (as per Curran et al. 2008). Showing these in Fig. 6, we see the expected increase in luminosity with redshift and note that our selection of the reddest PHFS sources (Sect.2.1) means that nearly all of our targets lie below $L_{\rm UV} = 10^{23}$ W Hz^{-1} (left panel). Since we are unlikely to detect molecular absorption in an environment not conducive to large columns of cool neutral gas, in the right panel of Fig. 6 we show the UV luminosity versus the *colour depth*, which we define as the optical–near-infrared colour normalised by the depth of the search. As expected from the column density—$V-K$ correlation (Fig. 4), this gives a vertical line with this quantity plotted as the abscissa[16] and from this definition we see that 20 discrete sources (mostly from this work) have been searched sufficiently deeply, of which only 12 are located in the bottom right quadrant defined by $L_{\rm UV} \lesssim 10^{23}$ W Hz^{-1} and a *colour depth* $\gtrsim 1$.

As expected, in Fig. 6 (right) there is an anti-correlation between the UV luminosity and $V-K$ colour, since the former is derived from the observed frame optical photometry. As such, there is also the possibility that the calculated values of $L_{\rm UV}$ are influenced by the dust extinction towards the source. However, the fact that 21-cm absorption is never detected above a critical luminosity (or below a critical magnitude/dust extinction), as well as the correlation between the 21-cm absorption strength and $V-K$ colour (Curran & Whiting 2010), indicates that the extinction occurs within the host in the case of the 21-cm detections, which follow the expected 50% detection rate for $L_{\rm UV} \lesssim 10^{23}$ W Hz^{-1} (Curran & Whiting 2010). Therefore, whether due to high intrinsic UV luminosities or a paucity of dust within the host galaxy, it remains that 21-cm absorption is not detected where $L_{\rm UV} \gtrsim 10^{23}$ W Hz^{-1} and where we do not detect 21-cm we do not expect to detect absorption by molecular gas.

Lastly, as well as a covering factor of $f \approx 1$, as per the four known systems, we have assumed an excitation temperature

---

[15] As well as a possible detection towards 1107–187, which at $z = 0.48909$ (Curran et al. 2011a), is not covered by the 76.88–77.12 GHz ($0.4947 < z_{\rm CO} < 0.4994$) range observed here (Fig. 2). 0213–026, 1504–166 and 1706+006 are undetected in 21-cm (Curran et al. 2011a), with the remainder of the sample as yet unsearched (see tables 1 & 2 of Curran & Whiting 2010).

[16] Adding the three intervening absorbers gives a *colour depth* of 1.00 ± 0.02 for both $N_{\rm CO}$ and $1000 \times N_{\rm HCO^+}$. The intervening absorbers are not shown in the plot as, although the ultra-violet luminosities can also be estimated, these are remote from the source.

Table 3. Summary of the millimetre-band scans towards 0500+019 with the Swedish ESO-Submillimetre Telescope (Murphy et al. 2003) in order of increasing frequency bands, as tabulated in Curran et al. (2005). We also show the results for 0727—155 since the emission redshift, $z_{\rm em}$, of the quasar is covered (by CO $1 \rightarrow 2$, where we show the fractional redshift range based upon $z = 1.547 - 1.591$). This is therefore included in our analysis (Fig. 5). The column density limits are calculated from the quoted optical depths per a 18 km s^{-1} (0500+019) and 70 km s^{-1} (0727–115) channel (Sect. 3.1), with $T_{\rm x} = 10$ K at $z = 0$.

Quasar	V	$z_{\rm em}$	HCO^{+}				CO			
			Trans.	z-range	$\Delta z/z_{\rm em}$	$N_{\rm total}$ [cm^{-2}]	Trans.	z-range	$\Delta z/z_{\rm em}$	$N_{\rm total}$ [cm^{-2}]
0500+019	21.2	0.58457	$0 \rightarrow 1$	0.1025–0.1391	0.063	$< 4.1 \times 10^{13}$	$0 \rightarrow 1$	0.4249–0.4722	0.081	$< 3.0 \times 10^{16}$
...	...	...	$0 \rightarrow 1$	0.0311–0.0431	0.021	$< 2.3 \times 10^{13}$	$0 \rightarrow 1$	0.3326–0.3482	0.027	$< 1.7 \times 10^{16}$
...	...	...	$1 \rightarrow 2$	0.5771–0.5846	0.013	$< 1.0 \times 10^{13}$	$0 \rightarrow 1$	0.0192–0.0283	0.016	$< 1.7 \times 10^{16}$
...	...	...	$1 \rightarrow 2$	0.2615–0.3721	0.189	$< 1.2 \times 10^{13}$	—	—	—	—
0727–115	22.5	1.591	$0 \rightarrow 1$	0.1025–0.1391	0.023	$< 4.3 \times 10^{13}$	$0 \rightarrow 1$	0.4249–0.4722	0.030	$< 3.2 \times 10^{16}$
...	...	...	$1 \rightarrow 2$	1.2049–1.2781	0.046	$< 1.7 \times 10^{13}$	—	—	—	—
...	...	...	$0 \rightarrow 1$	0–0.0630	0.040	$< 2.1 \times 10^{13}$	$0 \rightarrow 1$	0.2737–0.3739	0.063	$< 1.6 \times 10^{16}$
...	...	...	$1 \rightarrow 2$	0.9710–1.1260	0.097	$< 8.5 \times 10^{12}$	$1 \rightarrow 2$	1.5474–1.7478	0.027	$< 7.1 \times 10^{15}$
...	...	...	$1 \rightarrow 2$	0.2615–0.2926	0.020	$< 1.7 \times 10^{13}$	$1 \rightarrow 2$	0.6304–0.6706	0.025	$< 1.5 \times 10^{16}$
...	...	...	$2 \rightarrow 3$	0.8922–0.9388	0.029	$< 1.7 \times 10^{13}$	$2 \rightarrow 3$	1.4455–1.5058	0.038	$< 1.8 \times 10^{16}$
...	...	...	$3 \rightarrow 4$	1.5229–1.5850	0.039	$< 2.9 \times 10^{13}$	—	—	—	—
...	...	...	$1 \rightarrow 2$	0.2004–0.2491	0.031	$< 1.5 \times 10^{13}$	$1 \rightarrow 2$	0.5514–0.6144	0.040	$< 1.3 \times 10^{16}$
...	...	...	$2 \rightarrow 3$	0.8005–0.8737	0.046	$< 1.4 \times 10^{13}$	$2 \rightarrow 3$	1.3270–1.4215	0.059	$< 1.5 \times 10^{16}$
...	...	...	$3 \rightarrow 4$	1.4006–1.4981	0.061	$< 2.5 \times 10^{13}$	—	—	—	—

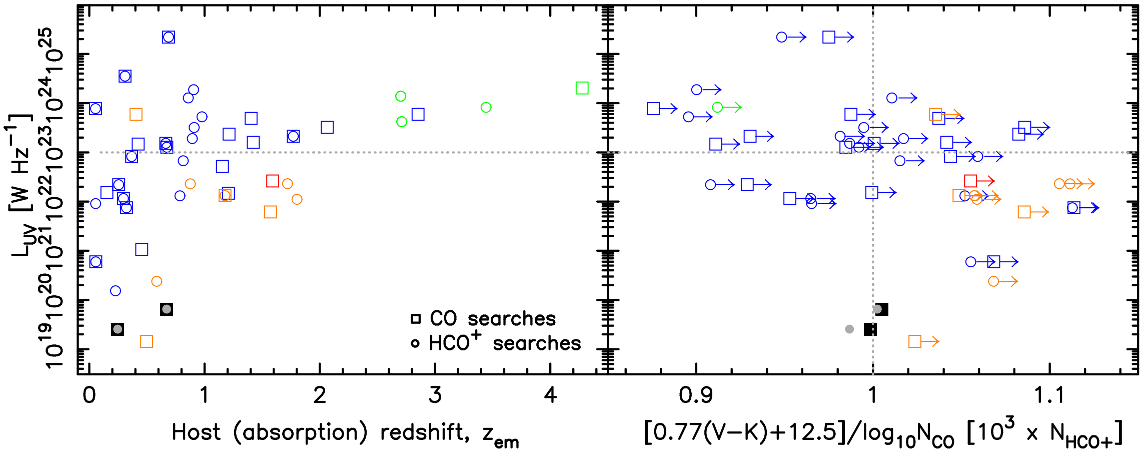

Figure 6. The ultra-violet ($\lambda \approx 1216$ Å) luminosity versus the redshift [left] and "*colour depth*" [right] for the sources listed in Table 4. The *colour depth* is defined by the fit to the CO column density–colour correlation for the four known systems (Fig. 5, left), i.e. $[0.77\,(V-K)+12.5]/\log_{10} N_{\rm CO}$ and $0.77\,(V-K)+12.5/\log_{10}(1000 \times N_{\rm HCO+})$, with the two known associated systems defining the vertical line at a value of 1.0. In the left panel we show all of the sources searched, as V and K magnitudes are not required, nor is the re-calculated 3σ r.m.s. noise required to be lower than the flux (as is not the case for the PKS 0422+004 searches nor HCO^{+} in Hydra A, Drinkwater et al. 1996). Note that, after the $\times 1000$ normalisation, the HCO^{+} points (shown in grey for clarity) are located close to the CO points for the two known associated systems.

of $T_{\rm x} \approx 10$ K (at $z = 0$) [Sect. 4.1]. Since there is no apparent correlation between the optical–near-infrared colour and the excitation temperature for the four known systems (Table 2)[17], we cannot estimate temperatures for any of the searched sample. If the gas were at higher excitation temperatures, being mostly observations of the lower rotational transitions (Table 3.1), the limits are less sensitive than quoted since a larger total column density would be required to give the same observed flux in these transitions. This has the effect of worsening the limits to the point where only two of the searched sources are (just) potentially detectable when $T_{\rm x} \approx 100$ K (Fig. 7), although if the gas is diffuse, such excitation temperatures may not be attainable, even in the presence of high kinetic temperatures.

5 SUMMARY

We have undertaken a survey for molecular absorption in the millimetre-band at high redshift. Like all previous surveys (since Wiklind & Combes 1995, 1996a,b, 1997), we have not detected millimetre-band spectral line absorption in any of the targets. In the case of absorption due to intervening sources, it has been established that the paucity of detections is due to the traditional optical selection of these objects, in which the redshift of the intervening object is usually known, biasing against the reddest, and thus dustiest, absorption complexes (Curran et al. 2006). We have therefore aimed to circumvent this bias, by searching for molecular absorption within the hosts of particularly red objects, although

---

[17] For 1413+135, $V-K = 4.81$ and $T_{\rm x} = 8$ K, similar to the excitation temperature of 1830−211 with $V-K = 6.25$.

Table 4. The magnitudes and calculated $\lambda \approx 1216$ Å luminosities [W Hz^{-1}] of the quasars and radio galaxies searched in millimetre-wave absorption. The bottom panel lists the two known associated absorbers.

Quasar	$z_{\rm em}$	Molecules	Ref	B	V	K	Refs	$\log_{10} L_{\rm UV}$
4C +40.01	0.255	CO, HCO$^+$	W96	17.89	17.67	14.87	Z04,S06	22.34
PKS 0113–118	0.672	CO, HCO$^+$	D96	18.27	17.95	14.37	Z04	23.11
PKS 0213–026	1.178	CO, HCO$^+$	C11	21.33	20.82	15.17	F00	22.12
[HB89] 0234+285	1.213	CO	W95	19.20	18.35	13.33	A09, S06	23.37
PKS 0335–122	3.442	HCN	D96	21.02	20.11	17.51	E05,H01	23.92
[HB89] 0422+004	0.310	CO, HCO$^+$, HCN	D96	13.89	14.12	11.31	F04	24.55
PKS 0434–188	2.702	HCO$^+$, HCN	C08	19.25	—	16.24	E05	24.14
PKS 0438–436	2.852	CO	D96	20.74	19.91	16.09	B04,E05	23.77
PKS 0446+11	1.207	CO	W96	21.43	20.36	15.37	A09,S06	22.17
PKS 0454+06	0.405	CO	C11	19.38	18.74	14.42	F00	21.57
PKS 0500+019	0.58457	HCO$^+$	C11	22.50	21.35	15.6	D97,C03,S96b	20.38
PKS 0521–365	0.0552	HCO$^+$	D96	15.60	14.60	11.33	H07,S06	21.96
PKS 0528+134	2.065	CO	W95	20.09	20.00	15.06	Z04,G00	23.51
[HB89] 0537–441	0.894	CO, HCO$^+$,HCN,CS	D96	17.93	17.34	13.02	F00	23.28
PKS 0601–17	2.711	HCO$^+$, HCN	C08	20.45	—	—	H01	23.66
CGRaBS J0650+6001	0.455	CO	W96	20.85	—	14.63	Z04,S06	21.03
PKS 0727–115	1.591	CO	M03	21.13	20.07	14.52	A09,C03	22.42
[HB89] 0735+178	0.424	CO	W95	16.30	15.68	13.03	A09,S06	23.17
PKS 0823-223	0.9103	HCO$^+$	W96	—	16.11	12.34	F93	23.51
Hydra A	0.0538	CO, HCO$^+$	D96	13.90	12.87	10.90	V91,C03	23.89
[HB89] 0954+658	0.368	CO, HCO$^+$	W96	17.18	16.80	12.43	P04,S06	22.92
PKS 1026–084	4.276	CO	C08	21.07	—	—	H01	24.31
PKS 1107–187	0.497	CO	C11	22.44	21.10	15.95	F00	19.16
FTM J1341+3301	1.720	HCO$^+$	C11	23.39	21.68	14.49	A09,G07	22.36
SBS 1347+539B	0.978	HCO$^+$	W96	17.95	17.52	15.07	A09,S06	23.72
[HB89] 1418+546	0.152	CO	W96	16.25	15.60	11.43	A09,S06	22.18
PKS 1430–155	1.573	CO	C11	22.50	23.24	17.50	D97,F00	21.79
3C 309.1	0.905	CO	W96	16.80	16.57	14.72	Z04,S06	24.27
PKS 1504–167	0.876	HCO$^+$	C11	20.28	19.75	14.01	F00	22.36
PKS 1548+056	1.422	CO	D96	19.37	18.65	14.30	F00	23.21
PKS 1555+001	1.77	CO, HCO$^+$	D96	20.34	19.95	16.24	F00	23.33
PKS 1622–253	0.786	HCO$^+$	W96	—	20.6	14.86	d94,S06	22.12
PKS 1622–29	0.815	HCO$^+$	W96	—	18.38	14.15	R02,S06	22.83
PKS 1725+044	0.296	CO, HCO$^+$	D96	17.92	17.46	14.13	F00	22.06
[HB89] 1749+096	0.322	CO, HCO$^+$	W96	17.98	17.39	12.00	O09,S06	21.87
[HB89] 1823+568	0.664	CO, HCO$^+$	W96	17.41	17.02	13.84	Z04,S06	23.18
Cygnus A	0.0561	CO, HCO$^+$	D96	17.04	15.52	10.28	V91,C03	20.78
CGRaB J2022+6136	0.228	HCO$^+$	W96	19.55	17.97	14.28	Z04,S06	20.19
[HB89] 2200+420	0.688	CO, HCO$^+$	W96	13.25	13.32	10.49	F04,S06	25.34
PKS 2223–052	1.404	CO	D96	18.59	18.33	14.69	F00	23.69
3C 454.3	0.859	HCO$^+$	W95	16.03	16.19	13.06	Z04,S06	24.11
PKS 2329–162	1.155	CO	D96	20.72	—	16.58	H01,W83	22.72
PKS 2337–334	1.802	HCO$^+$	C11	22.93	21.89	16.39	F00	22.05
PKS 1413+135	0.246710	CO, HCO$^+$, HCN, HNC	W97	21.37	19.74	14.93	A09,S06	19.41
B3 1504+377	0.67150	CO, HCO$^+$, HCN, HNC	W96	23.24	21.82	16.10	A09,S96a	19.81

Molecular search references: D96 – Drinkwater et al. (1996), W95 – Wiklind & Combes (1995), W96 – Wiklind & Combes (1996b), W97 – Wiklind & Combes (1997), M03 – Murphy et al. (2003), C08 – Curran et al. (2008), C11 – this paper.

Photometry references: W83 – Wright et al. (1983), F93 – Falomo et al. (1993), d94 – di Serego-Alighieri et al. (1994), S96a – Stickel et al. (1996a), S96b – Stickel et al. (1996b), D97 – Drinkwater et al. (1997), F00 – Francis et al. (2000), G00 – Ghosh et al. (2000), E01 – Ellison et al. (2001), H01 – SuperCOSMOS Sky Survey (Hambly et al. 2001), R02 – Romero et al. (2002), C03 – Cody & Braun (2003), B04 – Brocksopp et al. (2004), F04 – Fiorucci et al. (2004), P04 – Papadakis et al. (2004), Z04 – Zacharias et al. (2004), E05 – Ellison et al. (2005), S06 – 2MASS (Skrutskie et al. 2006), A09 – SDDS DR7(Abazajian et al. 2009), O09 – Ojha et al. (2009), FPC – P. Francis (priv. comm.).

like Drinkwater et al. (1996), who also targetted red sources (and type-2 AGN)[18], we find no absorption.

A possible reason for some of the non-detections is that only 12 of the 40 objects searched are known to be located in the bottom right quadrant of the ultra-violet luminosity–*colour depth* plot (Fig. 6, right), i.e. where $L_{\rm UV} \lesssim 10^{23}$ W Hz^{-1} and $[0.77\,(V-K)+12.5]/\log_{10}N_{\rm CO} \approx [0.77\,(V-K)+12.5]/\log_{10}(1000\times N_{\rm HCO+}) \gtrsim 1$. This suggests that only a dozen of the sources may

---

[18] Although as Curran & Whiting (2010) have shown, the bulk cool neutral gas (as traced by H I 21-cm absorption) is not located in the obscuring torus, invoked by unified schemes of active galactic nuclei.

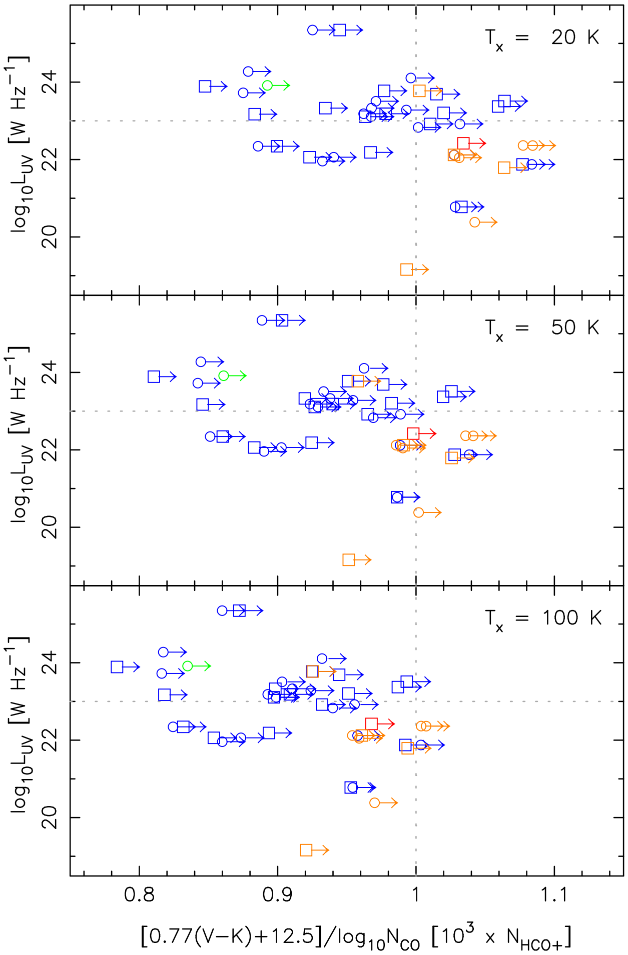

Figure 7. The *colour depth* distribution for various excitation temperatures.

be subject to an ultra-violet flux which permits the presence of cool neutral gas (Curran et al. 2008), while being "sufficiently red" to indicate the presence of a large column of dust along the sight-line to the quasar (Curran et al. 2006). Given that:

– For these, the reddening could be occuring anywhere along the line-of-sight, and not necessarily in the host galaxy, as is the case for three of the five known OH absorbers (four of which make up all the known redshifted millimetre-band absorbers). The only reason we chose to observe the emission redshift is that it gives a frequency to which to tune the receiver – Murphy et al. (2003); Curran et al. (2005) previously attempted millimetre-wave spectral scans towards very dim objects, but the redshift range scanned is a trade-off with the time spent on each frequency, resulting in poor optical depth limits over what were limited redshift ranges in only a few sources.

– This fifth absorber, which was detected in OH but not HCO$^+$, may be the result of lower millimetre-wave covering factors in comparison to those at decimetre wavelengths (Curran et al. 2007). This may be analogous to the effect seen in the optically selected DLAs (Sect. 1), where, due to the steeper cosmological evolution in the heavy element abundance in the H$_2$-bearing DLAs, Curran et al. (2004) suggest that these constitute a more homogeneous class of objects than the general population DLA (Prochaska et al. 2003). That is, H$_2$ absorption may only be observed in a limited subset of possible sight-lines and Zwaan & Prochaska (2006) suggest that a distinction could arise from the much smaller cross-section of the molecular gas, located in small and dense regions (e.g. Liszt & Lucas 1996), in comparison to that of the atomic gas. This means that only a narrow sight-line will occult the quasar, although the DLA may be apparent through the more widespread 21-cm absorption.

– As well as covering factor effects, if the excitation temperature of the putative absorbing gas is higher than the assumed $T_x = 10$ K (at $z = 0$), the column density limits are poorer than those calculated here. If large enough ($T_x \gtrsim 100$ K), none of these searches, mostly of the lower rotational transitions, have been sensitive enough to detect CO or HCO$^+$ absorption in these sources, although the absorbing medium may be too diffuse to reach such temperatures through collisional excitation.

Drinkwater et al. (1996) accounted for their non-detections by suggesting that the extinction may be occuring outwith the host galaxy or that the X-ray flux from the AGN may be photo-dissociating the molecules. These possibilities are similar to the points made above, although by quantifying these via the findings of Curran et al. (2006, 2008), we find that not all of the targets of Drinkwater et al. (1996) are sufficiently faint and reddened to have been detected, no matter the location of the obscuring material. Therefore, the key to finding new redshifted molecular absorbers in the millimetre-band is through the selection of the faintest optical objects (giving $L_{\rm UV} \lesssim 10^{23}$ W Hz^{-1}) and performing spectral scans towards these to *colour depth* limits of $\gtrsim 1$, as defined by the column densities and colours of the four known absorbers. In order to also circumvent the covering factor effect, pilot searches for OH in the decimetre band could be undertaken, with the low rest frequency (1667 MHz) allowing a full spectral scan in only four separate tunings with the Square Kilometre Array (Curran et al. 2004a).

ACKNOWLEDGEMENTS

We would like to thank A. Weiss for assisting with the IRAM observations, as well as Shigeru Takahashi, Jun Maekawa and Hiroki Ashizawa of Nobeyama Radio Observatory for their assistance in installing NEWSTAR and the data retrieval. MTM thanks the STFC for an Advanced Fellowship and the Australian Research Council for a QEII Research Fellowship (DP0877998).

We acknowledge financial support from the Access to Major Research Facilities Programme which is a component of the International Science Linkages Programme established under the Australian Government's innovation statement, Backing Australia's Ability.

This research has made use of the NASA/IPAC Extragalactic Database (NED) which is operated by the Jet Propulsion Laboratory, California Institute of Technology, under contract with the National Aeronautics and Space Administration. This research has also made use of NASA's Astrophysics Data System Bibliographic Services and ASURV Rev 1.2 (Lavalley et al. 1992), which implements the methods presented in Isobe et al. (1986).

Funding for the Sloan Digital Sky Survey (SDSS) and SDSS-II has been provided by the Alfred P. Sloan Foundation, the Participating Institutions, the National Science Foundation, the U.S. Department of Energy, the National Aeronautics and Space Administration, the Japanese Monbukagakusho, and the Max Planck Society, and the Higher Education Funding Council for England. The SDSS Web site is http://www.sdss.org/.

REFERENCES

Abazajian K. N., Adelman-McCarthy J. K., Agüeros M. A., et al., 2009, ApJS, 182, 543

Becker R. H., White R. L., Helfand D. J., 1995, ApJ, 450, 559

Brocksopp C., Puchnarewicz E. M., Mason K. O., Córdova F. A., Priedhorsky W. C., 2004, MNRAS, 349, 687

Carilli C. L., Menten K. M., Reid M. J., Rupen M. P., Yun M. S., 1998, ApJ, 494, 175

Carilli C. L., Perlman E. S., Stocke J. T., 1992, ApJ, 400, L13

Carilli C. L., Rupen M. P., Yanny B., 1993, ApJ, 412, L59

Chandra S., Kegel W. H., Roy R. J. L., Hertenstein T., 1995, A&AS, 114, 175

Chandra S., Maheshwari V. U., Sharma A. K., 1996, A&AS, 117, 557

Chengalur J. N., de Bruyn A. G., Narasimha D., 1999, A&A, 343, L79

Cody A. M., Braun R., 2003, A&A, 400, 871

Curran S. J., Darling J. K., Bolatto A. D., Whiting M. T., Bignell C., Webb J. K., 2007, MNRAS, 382, L11

Curran S. J., Kanekar N., Darling J. K., 2004a, Science with the Square Kilometer Array, New Astronomy Reviews 48. Elsevier, Amsterdam, pp 1095–1105

Curran S. J., Murphy M. T., Pihlström Y. M., Webb J. K., Bolatto A. D., Bower G. C., 2004b, MNRAS, 352, 563

Curran S. J., Webb J. K., Murphy M. T., Carswell R. F., 2004, MNRAS, 351, L24

Curran S. J., Webb J. K., Murphy M. T., Kuno N., 2005, in Engvold. O., ed., Highlights of Astronomy, Vol. 13, as presented at the XXVth General Assembly of the IAU - 2003 Deep searches for high redshift molecular absorption. ASP Conf. Ser., San Francisco, pp 845 – 847

Curran S. J., Whiting M., Murphy M. T., et al., 2011a, MNRAS, 413, 1165

Curran S. J., Whiting M., Murphy M. T., Webb J. K., Longmore S. N., Pihlström Y. M., Athreya R., Blake C., 2006, MNRAS, 371, 431

Curran S. J., Whiting M. T., 2010, ApJ, 712, 303

Curran S. J., Whiting M. T., Tanna A., Bignell C., Webb J. K., 2011b, MNRAS, 413, L86

Curran S. J., Whiting M. T., Wiklind T., Webb J. K., Murphy M. T., Purcell C. R., 2008, MNRAS, 391, 765

di Serego-Alighieri S., Danziger I. J., Morganti R., Tadhunter C. N., 1994, MNRAS, 269, 998

Drinkwater M. J., Combes F., Wiklind T., 1996, A&A, 312, 771

Drinkwater M. J., Webster R. L., Francis P. J., et al., 1997, MNRAS, 284, 85

Ellison S. L., Hall P. B., Lira P., 2005, AJ, 130, 1345

Ellison S. L., Yan L., Hook I. M., Pettini M., Wall J. V., Shaver P., 2001, A&A, 379, 393

Falomo R., Bersanelli M., Bouchet P., Tanzi E. G., 1993, AJ, 106, 11

Fiorucci M., Ciprini S., Tosti G., 2004, A&A, 419, 25

Francis P. J., Whiting M. T., Webster R. L., 2000, PASA, 17, 56

Fukugita M., Ichikawa T., Gunn J. E., Doi M., Shimasaku K., Schneider D. P., 1996, AJ, 111, 1748

Ghosh K. K., Ramsey B. D., Sadun A. C., Soundararajaperumal S., 2000, ApJS, 127, 11

Glikman E., Gregg M. D., Lacy M., Helfand D. J., Becker R. H., White R. L., 2004, ApJ, 607, 60

Hambly N., MacGillivray H., Read M., et al., 2001, MNRAS, 326, 1279

Isobe T., Feigelson E., Nelson P., 1986, ApJ, 306, 490

Jorgenson R. A., Wolfe A. M., Prochaska J. X., Carswell R. F., 2009, ApJ, 704, 247

Kanekar N., Carilli C. L., Langston G. I., et al., 2005, PhRvL, 95, 261301

Lavalley M. P., Isobe T., Feigelson E. D., 1992, in BAAS Vol. 24, ASURV, Pennsylvania State University. Report for the period Jan 1990 - Feb 1992.. pp 839–840

Liszt H., Lucas R., 1996, A&A, 314, 917

Murphy M. T., Curran S. J., Webb J. K., 2003, MNRAS, 342, 830

Noterdaeme P., Ledoux C., Petitjean P., Srianand R., 2008, A&A, 481, 327

Ojha R., Zacharias N., Hennessy G. S., Gaume R. A., Johnston K. J., 2009, AJ, 138, 845

Papadakis I. E., Samaritakis V., Boumis P., Papamastorakis J., 2004, A&A, 426, 437

Pickett H. M., Poynter R. L., Cohen E. A., Delitsky M. L., Pearson J. C., Müller H. S. P., 1998, J. Quant. Spectrosc. Radiat. Transfer, 60, 883

Prochaska J. X., Gawiser E., Wolfe A. M., Castro S., Djorgovski S. G., 2003, ApJ, 595, L9

Prochaska J. X., Herbert-Fort S., Wolfe A. M., 2005, ApJ, 635, 123

Romero G. E., Cellone S. A., Combi J. A., Andruchow I., 2002, A&A, 390, 431

Schneider D. P., Hall P. B., Richards G. T., et al., 2007, AJ, 134, 102

Skrutskie M. F., Cutri R. M., Stiening R., Weinberg M. D., Schneider S., Carpenter J. M., Beichman C., Capps R. . M., 2006, AJ, 131, 1163

Srianand R., Gupta N., Petitjean P., Noterdaeme P., Ledoux C., 2010, MNRAS, p. 1888

Srianand R., Noterdaeme P., Ledoux C., Petitjean P., 2008, A&A, 482, L39

Stickel M., Rieke G. H., Kühr H., Rieke M. J., 1996a, ApJ, 468, 556

Stickel M., Rieke M. J., Rieke G. H., Kühr H., 1996b, A&A, 306, 49

Wiklind T., Combes F., 1994, A&A, 286, L9

Wiklind T., Combes F., 1995, A&A, 299, 382

Wiklind T., Combes F., 1996a, Nat, 379, 139

Wiklind T., Combes F., 1996b, A&A, 315, 86

Wiklind T., Combes F., 1997, A&A, 328, 48

Wiklind T., Combes F., 1998, ApJ, 500, 129

Wright A., Otrupcek R., 1990, Parkes Catalogue. Australia Telescope National Facility

Wright A. E., Ables J. G., Allen D. A., 1983, MNRAS, 205, 793

Zacharias N., Monet D. G., Levine S. E., Urban S. E., Gaume R., Wycoff G. L., 2004, in Bulletin of the American Astronomical Society Vol. 36 of Bulletin of the American Astronomical Society, The Naval Observatory Merged Astrometric Dataset (NOMAD). p. 1418

Zwaan M. A., Prochaska J. X., 2006, ApJ, 643, 675

This paper has been typeset from a TEX/ LATEX file prepared by the author.